

A third-order field camera with microsecond resolution for MR system diagnostics

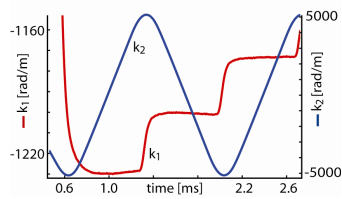
C. Barmet¹, B. J. Wilm¹, M. Pavan¹, and K. P. Pruessmann¹

¹Institute for Biomedical Engineering, University and ETH Zurich, Zurich, Zurich, Switzerland

Introduction: Most in-vivo MR procedures rely on dynamic gradient fields for signal preparation and encoding. They are often accompanied by undesired contributions that are not linear in space, namely of 0th order (B_0 eddy currents, field drifts, etc.), 2nd and 3rd order (concomitant fields, higher-order eddy currents, heating of shim irons, etc.). Assessing and minimizing such perturbations is a key objective in the development, calibration, maintenance, and quality assurance of MR systems. Therefore it is highly desirable to be able to simultaneously measure the full dynamics of fields of all relevant spatial orders. However, present-day field cameras (mostly based on NMR or the Hall effect) are limited to resolutions of about 1 ms [1],[2],[3]. Therefore the goal of the present work was to implement a 3rd-order NMR field camera with sufficient sensitivity to provide temporal resolution in the μ s range.

To illustrate the versatility of the resulting device, field dynamics have been studied in three specific situations: i) Mechanical vibrations of gradient coils, which cause field perturbations in the audiofrequency range and are a known confound in MR spectroscopy

Fig. 3: EPI readout (excerpt); time evolution of $k_{1,2}$



methods [4],[5]. ii) Field drifts during a demanding fMRI study. Requiring high gradient performance over long times such scans give rise not only to short-lived eddy currents, but also to long-term drifts due to thermal effects. Covering all relevant time scales from μ s to hours, the new field-camera readily lends itself to analyzing these effects comprehensively. iii) Field drifts following a long scan with demanding gradient duty cycle. Such drifts frequently affect subsequent scans.

Methods: The field camera consists of 16 NMR probes (H_2O doped with $CuSO_4$, 0.7 mm droplet diameter, 3-turn solenoid, SNR/BW = $4.8e4$ Hz) [6],[7], Fig. 6) equally distributed on a 20 cm sphere. The probes are operated in transmit/receive (T/R) mode and excited simultaneously by 4.5 μ s RF pulses generated by a separate transmit chain [7]. The resulting NMR signals are received via T/R switches with integrated preamplifiers and fed into 16 regular channels of the system spectrometer (3T Philips Achieva, Philips Healthcare, Best, NL). The miniaturized probe droplets tolerate gradient action up to $k_{max} = (350 \mu m)^{-1}$ without dephasing. Their signal lifetime is 150 ms, capturing field evolutions up to this duration with a single excitation. Longer-term dynamics can be observed by concatenating an arbitrary number of successive observations. For analysis, the phase of the probe data is fitted to a spatial model, using the 16 basis functions that constitute a full 3rd order, real-valued spherical harmonic expansion [8] (Tab. 1). The resulting dynamic phase coefficients reflect global phase error (k_0), the familiar k-space coordinates $k_1 = k_x$, $k_2 = k_y$, $k_3 = k_z$, as well as 2nd-order (k_4 - k_8) and 3rd-order (k_9 - k_{15}) order components. **Experiments:** i) Gradient coil vibrations and acoustic spectrum: each of the built-in gradient coils was separately driven at 31 mT/m for 900 ms and then switched off within 200 μ s. The ensuing fields were measured and studied in the time and frequency domains, including comparison with an acoustic spectrum obtained simultaneously with a microphone. ii) Following fMRI protocol was used as a test case: single-shot GRE EPI, 30 slices, 300 dynamics, TE = 35 ms, sequence TR = 100 ms, matrix = 92^2 ; total scan time = 15 min. The entire protocol was monitored with the field camera at a temporal resolution of 4.5 μ s. iii) Field drifts during 'cooling': after the fMRI scan, the magnetic field evolution in the idle scanner was observed for 50 min.

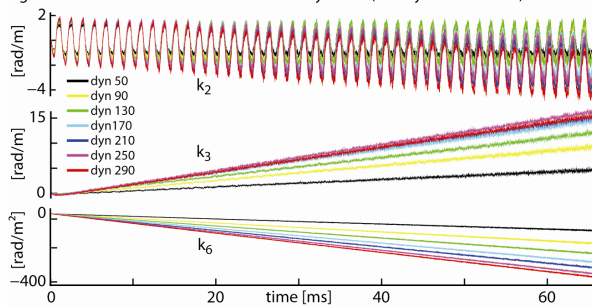
Tab. 1: spherical harmonics

nr.	basis function b_m
0	1
1	x
2	y
3	z
4	xy
5	yz
6	$3z^2 - (x^2 + y^2 + z^2)$
7	xz
8	$x^2 - y^2$
9	$3x^2y - y^3$
10	xyz
11	$y(5z^2 - (x^2 + y^2 + z^2))$
12	$5z^2 - 3z(x^2 + y^2 + z^2)$
13	$x(5z^2 - (x^2 + y^2 + z^2))$
14	$x^2z - y^2z$
15	$x^3 - 3xy^2$

Results: i) Figure 1 shows sample time evolutions of k_1 to k_3 following abrupt switching of the z gradient. While k_1 and k_2 appear to be affected only by eddy current effects, k_3 also exhibits a distinct oscillation (amplitude = 0.7 rad/m, decay-time = 15 ms) at 1335 Hz (Fig. 2). Moreover a very weak oscillation at 4109 Hz can be identified, which occurred mostly in k_1 and k_2 , but also in a third-order term (k_{11}). Both oscillation frequencies are also found in the acoustic spectrum (Fig. 2), confirming the mechanical nature of their origin. Switching the x and y gradients yielded multiple mechanical resonances.

ii) Figure 3 shows a brief excerpt of the phase coefficients k_1 (phase enc.) and k_2 (frequency enc.) during the first EPI readout, illustrating the necessity of very high temporal resolution. Magnetic field changes over time were identified by subtracting the coefficient time courses of the first dynamic scan from those of all following dynamics. Figure 4 shows the resulting drifts in temporal behavior of k_2 , k_3 , and k_6 for 7 different dynamics across the whole scan. k_2 : a fast oscillation driven by the frequency-encoding gradient is superimposed with a long-term drift. k_3 : the net drift in the phase accumulated under the read gradient amounts to 16 rad/m; interestingly it peaks after 12 min and then decreases again. k_6 : with a slowly saturating drift of 370 rad/m², this second-order contribution is appreciable. k_{12} (not shown): A linear 3rd order drift of 520 rad/m³ is still noticeable. Finally, a gradual change in the slope of k_0 (not shown) indicated a B_0 drift of -84 Hz over 15 min.

Fig. 4: coefficient drifts relative to the first dynamic (300 dyn over 15 min)



dynamics across many time scales (μ s to over an hour), up to 3rd order in space. This capability promises to render it a valuable tool for MR systems engineering and diagnostics. Besides the examples given in this work it could readily serve, e.g., for the assessment of gradient coils and amplifiers, fast pre-emphasis calibration, testing and tuning of higher-order shim systems, or the characterization of external field effects.

References: [1] Clark et al., J. Appl. Phys. 63:4185 (1988). [2] Hammer et al., Rev Sci Instrum 67(6):2378 (1996). [3] Keller, Metrolab Instruments, Geneva, Switzerland(2007) [4] Wu et al., MRM 44:532 (2000). [5] Nixon et al., JMR 192:209 (2008). [6] De Zanche et al., MRM 60:176 (2008). [7] Barmet et al., Proc. ISMRM 2008, p.1152. [8] Barmet et al., MRM 60:187 (2008).

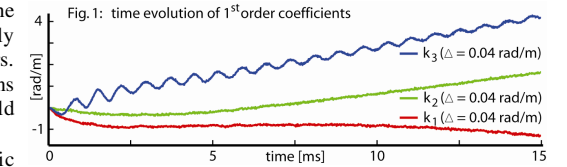


Fig. 2: acoustic and 1st order coefficients spectra after a sharp z-gradient slope

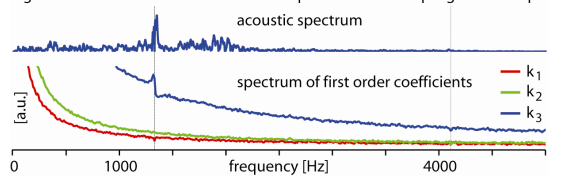


Fig. 6: 16 NMR probe field camera / schematic of probe-head

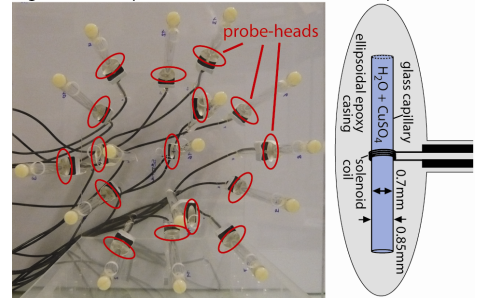
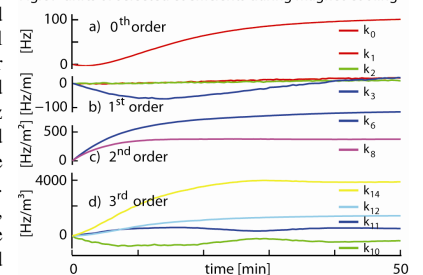


Fig. 5: drifts of selected coefficients during magnet 'cooling'



iii) The long-term measurement was evaluated in terms of frequencies (by taking the temporal derivatives of the phase coefficients). After decreasing by another 3 Hz, the main field displayed a positive drift by a total of 108 Hz (Fig. 5a). The gradient components varied much less; the z gradient (k_3) changed the direction of its drift only after 12 min (Fig. 5b). k_6 is the dominant 2nd order term (Fig. 5c), followed by k_8 . The 3rd order components were also appreciable and equally approached steady values within approximately 1 hour.

Conclusion: The described NMR field camera has been successfully used to observe field